

## TURBULENT CHANNEL FLOWS WITH SECONDARY MOTIONS: A CONCERTED DNS AND EXPERIMENTAL STUDY

L. von Deyn<sup>1</sup>, R. Örlü<sup>2</sup>, D. Gatti<sup>1</sup>, J. Kriegseis<sup>1</sup>, B. Frohnapfel<sup>1</sup> and A. Stroh<sup>1</sup>

<sup>1</sup>Department of Fluid Mechanics  
 Karlsruhe Institute of Technology  
 76131 Karlsruhe, Germany

von-deyn/ stroh/ davide.gatti/ jochen.kriegseis/ bettina.frohnapfel@kit.edu

<sup>2</sup>Linné FLOW Centre  
 KTH Mechanics  
 100 44 Stockholm, Sweden  
 ramis@mech.kth.se

### INTRODUCTION

Since the pioneering work of Hinze (1967) it is known that spanwise inhomogeneous surface structures can lead to the formation of large-scale secondary motions. In contrast to homogeneous roughness, whose effect is expected to be limited to the roughness layer (Flack *et al.*, 2007), the spanwise surface inhomogeneity results in spanwise-alternating low- and high-momentum flow pathways occupied by swirling secondary motions of Prandtl's second kind (Anderson *et al.*, 2015).

The turbulent secondary flows are known to alter important flow quantities such as the streamwise velocity and the skin-friction drag (Medjnoun *et al.*, 2018). The present contribution aims at analyzing large-scale secondary motions both numerically and experimentally in a channel-flow configuration, allowing a meaningful comparison of the two approaches.

To this aim, first turbulence measurements from a channel flow facility are obtained in order to establish the flow quality and its canonical behaviour, as well as ascertain that the chosen measurement technique resolves the energy of the relevant scales. Finally, a heterogeneous geometry consisting of streamwise strips of elevated smooth surfaces (of height  $h = 0.08 \delta$ ) mounted at a spanwise spacing of  $S = 1.24 \delta$  is studied, where  $\delta$  denotes the channel-half height as depicted in Fig. 1. This configuration is expected to generate a pronounced secondary motion of Prandtl's second kind. Global parameters such as the skin-friction coefficient and the streamwise velocity are measured with a liaison of hot-wire and pressure-drop measurements and compared to the fully resolved statistics of a direct numerical simulation (DNS) at matched Reynolds number.

### EXPERIMENTAL AND NUMERICAL DETAILS

A schematic of both the experimental and numerical setup is depicted in Fig. 2. The experimental facility consists of an open-circuit blower tunnel developed by Güttler (2015). It allows the measurement of small changes in skin-friction drag by evaluating the static pressure at 21 pressure taps located along both side walls of a  $314 \delta$  long channel

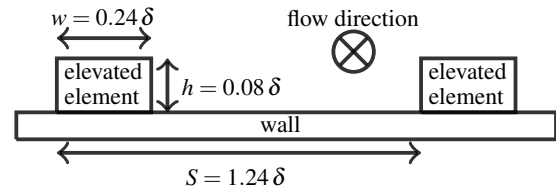


Figure 1: Surface parameters, with  $\delta$  denoting the channel-half height.

test section with an aspect ratio of 12. The test section is divided into three segments of  $76 \delta$ ,  $119 \delta$  and  $119 \delta$  streamwise extents. In the present investigation the last segment is equipped with 19 elevated streamwise-aligned ridges with the characteristics shown in Fig. 1 on the upper and lower side of the test section.

A hot-wire probe is used to measure the streamwise velocity at different wall-normal and spanwise positions. The streamwise location of the measurement campaign was fixed to one centimeter upstream of the test section outlet, since measurements showed that first and second-order statistics were identical with those measured further upstream up to 15 cm upstream of test section outlet. The probe consists of a single hot-wire and is of boundary-layer type (replicating a DANTEC 55P15) with a  $2.5 \mu\text{m}$  diameter Platinum wire and a sensing length of about 0.5 mm, resulting in an inner-scaled wire length of  $L^+ \approx 20$  at a friction Reynolds number of  $Re_\tau = \frac{u_\tau \delta}{\nu} \approx 550$ . This length was deemed sufficient to adequately resolve the turbulence statistics (Hutchins *et al.*, 2009). Prior to utilizing this probe a DANTEC boundary-layer type 55P05 with a (modified) active wire length of 3 mm was used in order to perform an extensive, long-time mean flow characterization, without the need for frequent re-calibrations. Results from this probe will be shown as part of the flow-quality assessment.

A DANTEC Streamline Pro frame in conjunction with a 90C10 constant temperature anemometer (CTA) system is used and operated at fixed overheat ratio of 80 %. Turbulence statistics were acquired with a sampling time and acquisition frequencies between 10s and 60s and 60kHz

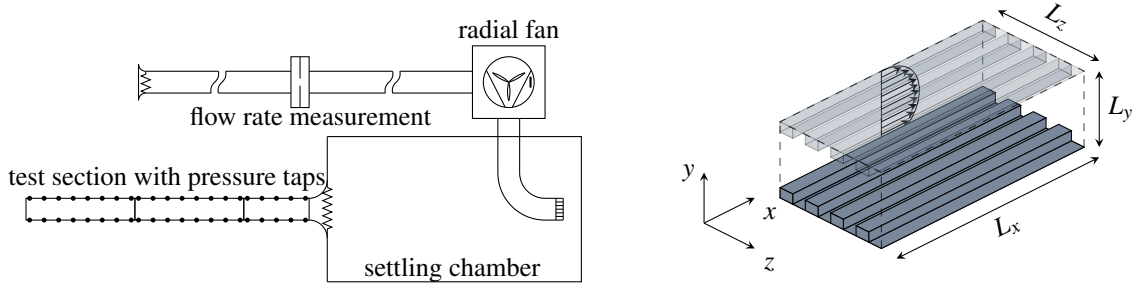


Figure 2: Experimental facility (left) vs. numerical setup (right).

down to 20kHz, respectively, depending on  $Re$ . The measurement grid for the wall-normal/spanwise characterization, on the other hand, as will be discussed in Fig. 7 consists of up to 3000 measurement points, each with an acquisition time of 5 s and a sampling rate of 60kHz. An offset and gain was applied to the top of the bridge voltage in order to match the voltage range of the 16-bit A/D converter used. In order to avoid aliasing at the higher velocities, an in-built analog low-pass filter was set up at the Nyquist frequency prior to data acquisition.

At the same time, direct numerical simulations (DNS) of a fully developed turbulent channel flow in a smooth and structured configuration replicating the experiment are carried out under a constant flow rate condition. The code implementation is based on the pseudo-spectral solver with Fourier expansions in the streamwise ( $x$ ) and spanwise ( $z$ ) directions and Chebyshev polynomials in the wall-normal direction ( $y$ ) (Chevalier *et al.*, 2007). Periodic boundary conditions are employed in streamwise and spanwise directions such that the in contrast to the experiment the DNS set-up does not contain any side walls. The required surface structuring is implemented with an immersed boundary method (Goldstein *et al.*, 1993).

After having characterized the surface employed in the experiment using photogrammetry (Hallert, 1960) an adequate representation of the structure geometry in the simulation was achieved by rounding the upper corners of the elevated element with a radius of  $0.02 \delta$  as depicted in Figs. 8. Details on the numerical procedure are outlined in Forooghi *et al.* (2018) and information regarding simulation domain and resolution for the present case are presented in table 1. Temporal and spatial averaging in the streamwise direction is applied to the DNS results, since the secondary motion is observed in the cross sectional plane perpendicular to the main flow direction. The bulk Reynolds number  $Re_b$  for the comparison of hot-wire experimental and numerical data is set to  $Re_b = 1.8 \times 10^4$ , which corresponds to a friction Reynolds number of  $Re_\tau \approx 550$ .

## FLOW QUALITY

While the present open-circuit blower tunnel has extensively been used and validated in terms of pressure drop

Table 1: Numerical properties of the DNS.

$N_x \times N_y \times N_z$	$L_x \times L_y \times L_z$	$\Delta x^+ \times \Delta y_{min}^+ \times \Delta z^+$
$768 \times 385 \times 384$	$8 \delta \times 2 \delta \times 3.72 \delta$	$5.7 \times 0.02 \times 5.3$

measurements, i.e. skin-friction coefficient and mean flow quantities (Güttler, 2015; Gatti *et al.*, 2015), turbulence statistics have not been presented previously. The present section therefore compiles a number of hot-wire anemometry results in order to verify that the fully developed turbulent channel flow established adheres to canonical results reported in the literature. To this end, Fig. 3 collects 9 independent measurements obtained from a (modified) DANTEC boundary-layer type (55P05) of probe (5 micron diameter and 3 mm active length) as well as a in-house built miniature replica of it with a reduced wire length (2.5 micron and 0.5 mm) that were obtained over a period of 2 month. As apparent from the grey symbols, showing all measurement points at the nominal Reynolds number of  $Re_b = 18000$ , the results agree well with the DNS by Hoyas & Jiménez (2008) at a matched  $Re$  which coincide with the present DNS results for the smooth-wall case. The relative standard deviation of these measurements is limited to  $\pm 0.5\%$  throughout the channel as apparent from the error bars (in red).

The requirement to utilize miniaturized boundary-layer probes for the present channel flow dimensions becomes acute when considering the variance profiles. Out of 9 profiles 3 were acquired with the modified 55P05 DANTEC

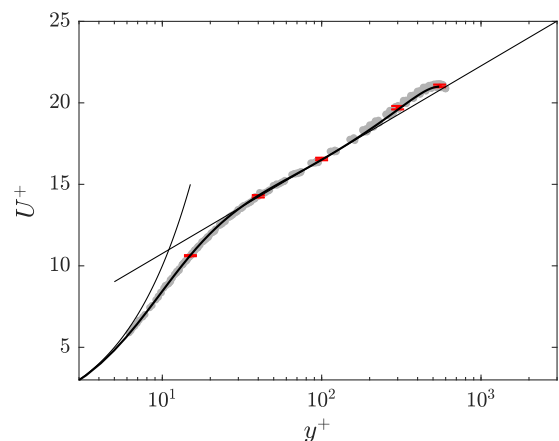


Figure 3: Inner-scaled mean streamwise velocity profiles for  $Re_b = 18000$ . Grey symbols depict measurements from 9 independent profile scans, while red error bars indicate the standard deviation at  $y^+ = 15, 40, 100, 300$  and  $550$ . Black solid line represents the DNS by Hoyas & Jiménez (2008) at a matched  $Re_\tau = 550$ . Thin black lines represent the linear and logarithmic velocity profile.

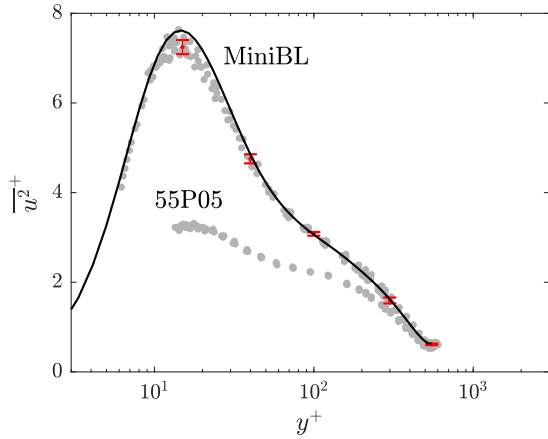


Figure 4: Inner-scaled variance profiles of the streamwise velocity component for the same cases as depicted in Fig. 3, with 3 and 6 profiles from the miniaturized boundary-layer probe (MiniBL) and (modified) 55P05. For symbols see caption of Fig. 3.

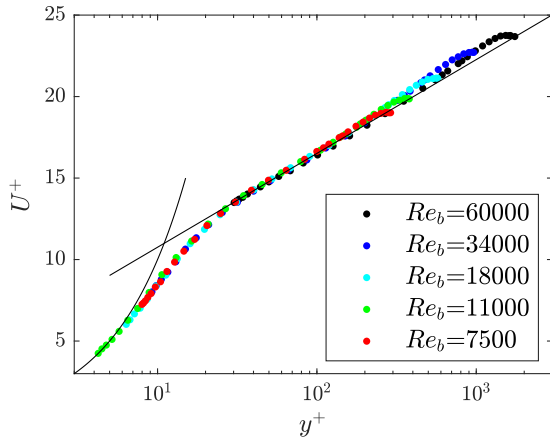


Figure 5: Inner-scaled mean streamwise velocity profiles for the Reynolds number range  $7500 \leq Re_b \leq 60000$ .

probe, which for the present  $Re$  has an inner-scaled active wire length of  $L^+ = 125$ , which measures a strongly attenuated velocity signal; note that a standard 55P15 with its 1.25 mm active wire length would still yield a  $L^+$  of 50, thereby emphasizing the need for the present miniaturized boundary-layer probe. Henceforth, only results from the in-house build miniature (henceforth MiniBL) probe will be considered. Their deviation from each other is in this case still limited to  $\pm 2\%$  and agrees also in this case with the DNS data by Hoyas & Jiménez (2008), with a weak underestimation for the near-wall peak in accordance with Segalini *et al.* (2011).

Based on the aforementioned good agreement between experiments and simulation, the channel flow has also been characterized over the range  $7500 \leq Re_b \leq 60000$ , which exhibits a good collapse of the profiles within the inner layer as shown in figure 5. In addition to the velocity profiles, Fig. 6 shows the resulting overall flow resistance in terms of the skin-friction coefficient. In this respect it is important to note the difference between local and global quantities. The mean and variance profiles shown in Fig. 3–5 are normalized with the friction velocity obtained through a fit

of the data measured within the buffer region (Örlü *et al.*, 2010), since the direct skin-friction measurements through the pressure drop represent a spanwise average (bulk) value and are dependent on the aspect ratio of the channel.

The results from the present pressure-drop measurements are an excellent agreement with the correlation proposed by Dean (1978) as can be seen in figure 6 (blue symbols). The skin-friction coefficient from the DNS on the other hand depicts an apparent discrepancy, which is also associated with the difference between local and global values. This has been investigated in more recent studies (Vinueza *et al.*, 2015) and the slightly smaller value compared to the experiments ( $\Delta C_f < 5\%$ ) can be traced back to the lack of the sidewalls in the DNS compared to the present channel flow with an aspect ratio of 12.

## DISCUSSION

The global skin friction drag for the flow with secondary motion as a function of Reynolds numbers is shown in figure 6 in comparison to the smooth wall reference. The different symbols in the plot indicate different techniques for the flow rate measurement in the wind tunnel (inlet nozzle vs. orifice flow meter) which show a slight systematic off-set in the data. As expected, the structured wall shows an increased skin friction drag compared to the smooth wall. The secondary motions lead to a significant increase of around 15% in skin-friction drag, which is comparable to the values reported by e.g. Medjnoun *et al.* (2018).

Especially in the higher Reynolds-number range the  $C_f$  vs  $Re_b$ -curves appear to develop parallel to each other. This indicates that the structured surface does not reach a fully rough state in the presently investigated Reynolds number range. Such a result is not surprising as the streamwise ridges do not introduce any pressure drag. However, flows with secondary motions generated by stripes of roughness, which introduce pressure drag, might show a different behavior in this respect.

The agreement between experimental and DNS results is better for the structured surface than for the smooth one. As discussed before, the off-set between experiments and DNS is related to the missing side-walls in the DNS. As the relevance of the skin-friction drag on the side walls decreases with increasing skin friction drag on the top and bottom walls the observed trend is reasonable.

Figure 7 shows the time averaged streamwise velocity  $\bar{U}$  obtained by the hot-wire measurements over 3 spanwise spacings of the strips in the spanwise/wall-normal plane. The underlying grid in the figures visualized the measurement locations. The clearly visible bulges are a consequence of the secondary motions. The long-time steadiness of the channel flow as well as the quality of the surface strips is clearly evident from the spanwise homogeneity of the velocity measurements. A comparison of the experimental data set with the DNS results is shown in a phase averaged manner in Fig. 8. The depicted contour lines of streamwise mean velocity  $\bar{U}$  from both experiments and simulations collapse well indicating a consistent generation and acquisition of the secondary motions in both physical and numerical experiments. The mean secondary flow in the plane normal to the streamwise flow direction is visualized based on the DNS results (grey arrows): low momentum pathways are located above the ridges and high momentum pathways above the valleys.

The premultiplied streamwise energy spectra obtained

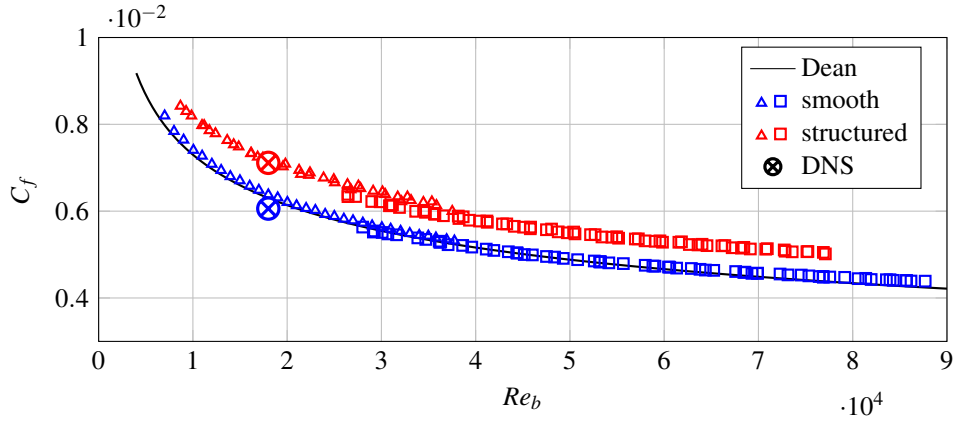


Figure 6: Comparison of the skin-friction factor  $C_f$  for smooth and structured surface. Various markers denote different flow rate measurement techniques.

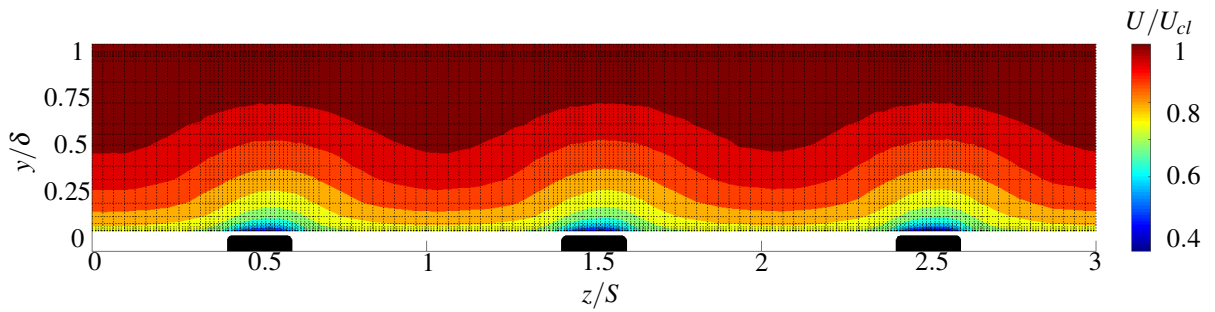


Figure 7: Time averaged streamwise velocity  $U$  obtained from hot-wire experiments. Intersection of dashed lines indicate the measurement grid.

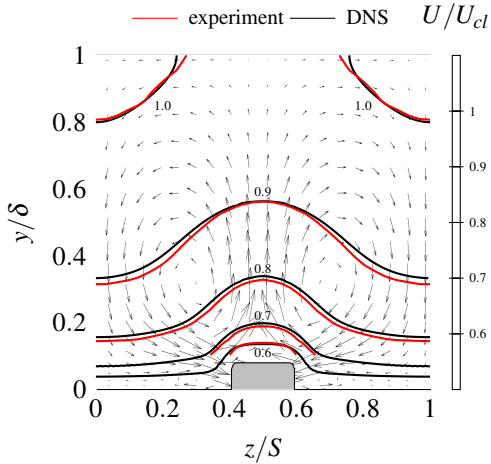


Figure 8: Phase averaged mean streamwise velocity contours for experimental and DNS data sets with arrows representing secondary motion (DNS data).

from two measurements at different Reynolds numbers ( $Re_b = 18000$  and  $Re_b = 60000$ ) and DNS at the lower Reynolds number ( $Re_b = 18000$ ) are shown in Figures 9, 10 and 11, respectively. Due to the difficulty to measure the local friction velocity in the structured channel, the spectra are compared in outer units. The comparison between the smooth wall experiment and DNS at the same Reynolds number (Fig. 9 left vs. Fig. 11 left) demonstrates that the hot-wires indeed resolve all relevant scales of the flow. Note that the spectra from the DNS data are obtained by consid-

ering the streamwise variations of the flow which are then translated into temporal variations based on the Taylor hypothesis using  $f = \bar{U}/\lambda_x$ , where  $\lambda_x$  is the streamwise wavelength and  $f$  is the frequency.

The experimentally obtained spectra in the flow with ridges show the emergence of an outer peak above the ridge in comparison to the smooth reference at both Reynolds numbers (Fig. 9 and 10 middle) as was also observed by Wangsawijaya *et al.* (2018); a clear indication of an energized outer layer. This effect appears to be more pronounced at higher Reynolds number. A similar outer peak has been observed also in channels and turbulent boundary layers with wall blowing Kametani *et al.* (2015). This outer peak is not found in the region of high momentum pathways in the valleys between the ridges.

The DNS data is used to obtain a complementary pre-multiplied streamwise energy spectra based on integration over the entire channel width, as shown in Fig. 11. In this visualization the position of the structure tips at  $y = 0.08\delta$  is clearly visible. A strong outer peak just above  $y = 0.08\delta$  gives the visual impression of a second near-wall peak in respect to the ridge surface.

## CONCLUSIONS

The turbulent channel flow with streamwise aligned ridges has been investigated in a concerted experimental and numerical study. Based on hot-wire measurement with miniature probes the flow quality of the experimental facility of a channel flow with aspect ratio 12 is documented. The integral pressure drop measurement of the facility shows a very good agreement with literature data

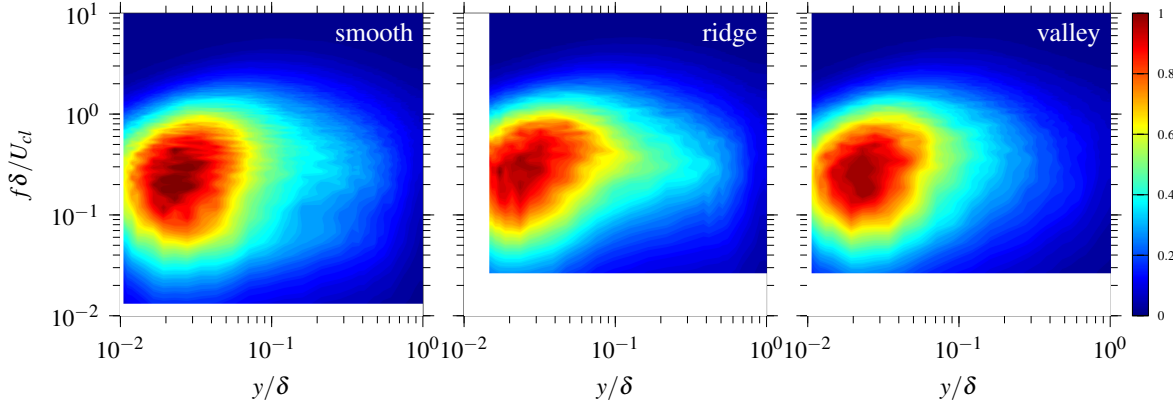


Figure 9: Contour map of the premultiplied streamwise energy spectra at  $Re_b = 18000$  in outer units (normalized through  $\delta$  and  $U_{\delta l}$ ) measured for the smooth channel (left), in the center of the ridge (middle) and in the center of the valley (right).

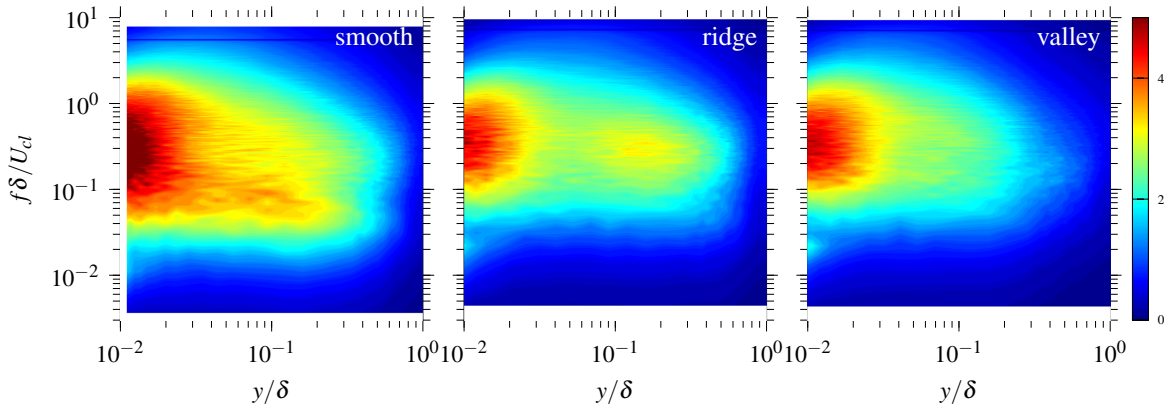


Figure 10: Contour map of the premultiplied streamwise energy spectra at  $Re_b = 60000$  in outer units (normalized through  $\delta$  and  $U_{\delta l}$ ) measured for the smooth channel (left), in the center of the ridge (middle) and in the center of the valley (right).

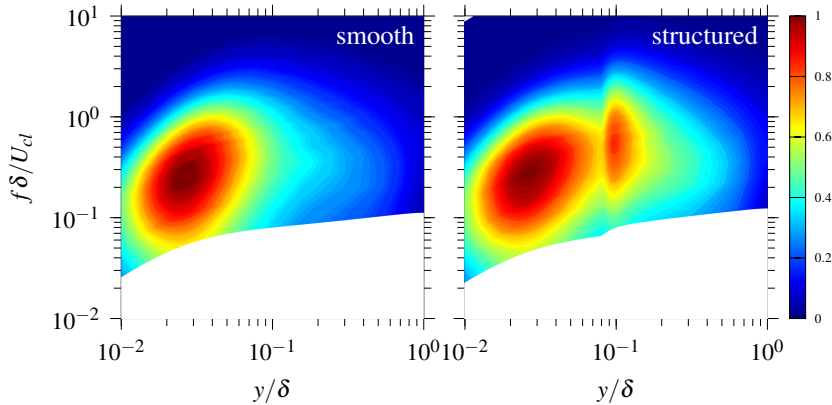


Figure 11: Contour map of the premultiplied streamwise energy spectra at  $Re_b = 18000$  in outer units (normalized through  $\delta$  and  $U_{\delta l}$ ) from the DNS of a smooth channel (left) and structured channel (right).

over a wide Reynolds number range. The insertion of streamwise-aligned ridges into the channel yields a significant drag increase which is caused by the increase of the wetted surface area and the occurrence of secondary motions of Prandtl's second kind. It is found that the increased  $C_f$  value for the rough wall maintains the decreasing trend with increasing Reynolds number indicating that this sur-

face does not reach a fully rough state in the investigated Reynolds number range which is reported to be reached e.g. for riblets in the literature (Jiménez, 2004). The comparison of the experimental mean flow field shows excellent agreement with the DNS data at the same Reynolds number ( $Re_b = 18000$ ). The DNS data allows to visualize the corresponding secondary motion which features low momentum

pathways above the ridges and high momentum pathways in the valleys in between. Higher order statistics between experiment and DNS are also in very good agreement which is documented through the premultiplied streamwise energy spectra. Those show the appearance of a secondary peak in the region of low momentum pathways as previously reported by Medjnoun *et al.* (2018) and Wangsawijaya *et al.* (2018). This peak appears to strengthen as the Reynolds number increases. The spanwise integrated energy spectrum based on the DNS data reveals a strong frequency peak in the region slightly above the ridges which might be understood as a near-wall peak above the ridge surface.

### Acknowledgement

This work is supported by the Priority Programme SPP 1881 Turbulent Superstructures of the Deutsche Forschungsgemeinschaft. Computing time has been provided by the computational resource ForHLR Phase I & II funded by the Ministry of Science, Research and the Arts Baden-Württemberg and DFG (Deutsche Forschungsgemeinschaft).

### REFERENCES

- Anderson, W., Barros, J. M., Christensen, K. T. & Awasthi, A. 2015 Numerical and experimental study of mechanisms responsible for turbulent secondary flows in boundary layer flows over spanwise heterogeneous roughness. *J. Fluid Mech.* **768**, 316–347.
- Chevalier, M., Schlatter, P., Lundbladh, A. & Henningson, D. S. 2007 Simson – A pseudo-spectral solver for incompressible boundary layer flows. *Tech. Rep.* TRITA-MEK 2007-07. KTH Stockholm, Stockholm, Sweden.
- Dean, R. 1978 Reynolds number dependence of skin friction and other bulk flow variables in two-dimensional rectangular duct flow. *ASME. J. Fluids Eng* **100**, 215–223.
- Flack, K. A., Schultz, M. P. & Connelly, J. S. 2007 Examination of a critical roughness height for outer layer similarity. *Phys. Fluids* **19**, 095104.
- Forooghi, P., Stroh, A., Schlatter, P. & Frohnepfel, B. 2018 Direct numerical simulation of flow over dissimilar, randomly distributed roughness elements: A systematic study on the effect of surface morphology on turbulence. *Phys. Rev. Fluids* **3**, 044605.
- Gatti, D., Güttler, A., Frohnepfel, B. & Tropea, C. 2015 Experimental assessment of spanwise-oscillating dielectric electroactive surfaces for turbulent drag reduction in an air channel flow. *Exp. Fluids* **56** (5), 110.
- Goldstein, D., Handler, R. & Sirovich, L. 1993 Modeling a no-slip flow boundary with an external force field. *J. Comput. Phys.* **105** (2), 354–366.
- Güttler, A. 2015 High accuracy determination of skin friction differences in an air channel flow based on pressure drop measurements. PhD thesis, Karlsruhe Institute of Technology.
- Hallert, B. 1960 *Photogrammetry, basic principles and general survey*. McGraw-Hill.
- Hinze, J. O. 1967 Secondary currents in wall turbulence. *Phys. Fluids* **10**, 122–125.
- Hoyas, S. & Jiménez, J. 2008 Reynolds number effects on the reynolds-stress budgets in turbulent channels. *Phys. Fluids* **20**, 101511.
- Hutchins, N., Nickels, Timothy B, Marusic, I & Chong, MS 2009 Hot-wire spatial resolution issues in wall-bounded turbulence. *J. Fluid Mech.* **635**, 103–136.
- Jiménez, J. 2004 Turbulent flows over rough walls. *Ann. Rev. Fluid Mech.* **36** (1), 173–196.
- Kametani, Y., Fukagata, K., Örlü, R. & Schlatter, P. 2015 Effect of uniform blowing/suction in a turbulent boundary layer at moderate reynolds number. *Int. J. Heat Fluid Flow* **55**, 132–142.
- Medjnoun, T., Vanderwel, C. & Ganapathisubramani, B. 2018 Characteristics of turbulent boundary layers over smooth surfaces with spanwise heterogeneities. *J. Fluid Mech.* **838**, 516–543.
- Örlü, R., Fransson, J. H. M. & Alfredsson, P. H. 2010 On near wall measurements of wall bounded flowsthe necessity of an accurate determination of the wall position. *Prog. Aerosp. Sci.* **46**, 353–387.
- Segalini, A., Örlü, R., Schlatter, P., Alfredsson, P. H., Rüedi, J.-D. & Talamelli, A. 2011 A method to estimate turbulence intensity and transverse taylor microscale in turbulent flows from spatially averaged hot-wire data. *Exp. Fluids* **51**, 693.
- Vinuesa, R., Schlatter, P. & Nagib, H. M. 2015 On minimum aspect ratio for duct flow facilities and the role of side walls in generating secondary flows. *J. Turbulence* **16**, 588–606.
- Wangsawijaya, D., de Silva, C., Baidya, R., Chung, D., Marusic, I. & Hutchins, N. 2018 Secondary flow over surfaces with spanwise heterogeneity. *Proceedings of 21st Australasian Fluid Mechanics Conference* .